VILNIUS UNIVERSITY
CENTER FOR PHYSICAL SCIENCES AND TECHNOLOGY
SEMICONDUCTOR PHYSICS INSTITUTE

GEDIMINAS ŠLEKAS

INVESTIGATION OF ELECTRODYNAMIC PROPERTIES OF SMALL SCALE OBJECTS USING FINITE-DIFFERENCE TIME-DOMAIN METHOD

Summary of doctoral dissertation
Physical sciences, physics (02 P), semiconductor physics (P 265)

Vilnius, 2014

Doctoral dissertation prepared 2009 – 2014 at the Microwave laboratory of Center for Physical Sciences and Technology.

Scientific supervisor:

habil. dr. Žilvinas Kancleris (Center for Physical Sciences and Technology, Physical sciences, physics – 02P, semiconductor physics – P265)

Council of defence of the doctoral dissertation of Physical Sciences at Vilnius University:

Chairman:

prof. habil. dr. Gintaras Valušis (Center for Physical Sciences and Technology, Physical sciences, physics – 02P, semiconductor physics – P265)

Members:

prof. habil. dr. Antanas Čenys (Vilnius Gediminas Technical University, Physical sciences, physics – 02P, semiconductor physics – P265)

prof. dr. habil. Algirdas Sužiedėlis (Center for Physical Sciences and Technology, Physical sciences, physics – 02P, semiconductor physics – P265)

prof. habil. dr. Gintautas Tamulaitis (Vilnius University, Physical sciences, physics – 02P, semiconductor physics – P265)

prof. dr. Vytautas Urbanavičius (Vilnius Gediminas Technical University, technological sciences, electrical and electronics engineering – 01T, high frequency technology, microwaves – T191)

Opponents:

dr. Ramūnas Adomavičius (Center for Physical Sciences and Technology, Physical sciences, physics – 02P, semiconductor physics – P265)

doc. dr. Mečislavas Meilūnas (Vilnius Gediminas Technical University, Physical sciences, mathematics – 01P, computer science, numerical methods, systems, control - P170)

The official defence of doctoral dissertation will be held in public session of Vilnius university Defence Council of Physical sciences at 15 h. on 19 September 2014 in the Conference hall of the Semiconductor Physics Institute (Center for Physical Sciences and Technology), A. Goštauto 11, LT – 01108 Vilnius, Lithuania.

The summary of the doctoral dissertation has been distributed on 25 July 2014.

The doctoral dissertation is available at the libraries of Vilnius University and Center for Physical Sciences and Technology.

VILNIAUS UNIVERSITETAS
FIZINIŲ IR TECHNOLOGIJOS MOKSLŲ CENTRAS
PUSLAIDININKIŲ FIZIKOS INSTITUTAS

GEDIMINAS ŠLEKAS

MAŽŲ MATMENŲ OBJEKTŲ ELEKTRODINAMINIŲ SAVYBIŲ TYRIMAS BAIGTINIŲ SKIRTUMŲ LAIKO SKALĖJE METODU

Daktaro disertacija
Fiziniai mokslai, fizika (02P), puslaidininkių fizika (P265)

Vilnius, 2014

Disertacija rengta 2009 – 2014 metais Fizinių ir Technologijos Mokslo Centro Puslaidininkių fizikos instituto Mikrobangų laboratorijoje.

Mokslinis vadovas:
habil. dr. Žilvinas Kancleris (FTMC Puslaidininkių fizikos institutas, fiziniai mokslai, fizika – 02P, puslaidininkių fizika – P265)

Disertacija ginama Vilniaus universiteto Fizikos mokslo krypties taryboje

Pirmininkas:

prof. habil. dr. Gintaras Valušis (Fizinių ir technologijos mokslų centras, fiziniai mokslai, fizika – 02P, puslaidininkių fizika – P265)

Nariai:

prof. habil. dr. Antanas Čenys (Vilniaus Gedimino technikos universitetas, fiziniai mokslai, fizika – 02P, puslaidininkių fizika – P265)

prof. dr. habil. Algirdas Sužiedėlis (Fizinių ir technologijos mokslų centras, fiziniai mokslai, fizika – 02P, puslaidininkių fizika – P265)

prof. habil. dr. Gintautas Tamulaitis (Vilniaus universitetas, fiziniai mokslai, fizika – 02P, puslaidininkių fizika – P265)

prof. dr. Vytautas Urbanavičius (Vilniaus Gedimino technikos universitetas, technologiniai mokslai, elektros ir elektronikos inžinerija – 01T, aukštų dažnių technologijos, mikrobangos – T191)

Oponentai:

dr. Ramūnas Adomavičius (Fizinių ir technologijos mokslų centras, fiziniai mokslai, fizika – 02P, puslaidininkių fizika – P265)
doc. dr. Mečislavas Meilūnas (Vilniaus Gedimino technikos universitetas, fiziniai mokslai, matematika – 01P, kompiuterių mokslas, skaitiniai metodai, sistemos, valdymas - P170)

Disertacija bus ginama viešame Fizikos mokslo krypties tarybos posėdyje 2014 m. rugsėjo 19 d. 15 val. Fizinių ir technologijos mokslų centro Puslaidininkių fizikos instituto posėdžių salėje, A. Goštauto g. 11, LT-01108 Vilnius, Lietuva.

Disertacijos santrauka išsiuntinėta 2014 m. liepos 25 d.

Disertaciją galima peržiūrėti Vilniaus universiteto, bei Fizinių ir technologijos mokslų centro bibliotekose.

List of abbreviations

2DEG	Two-dimensional electron gas
CPU	Central processing unit
CUDA	Compute Unified Device Architecture
EM	Electromagnetic
FDTD	Finite-difference time-domain
FPR	Fabry-Perot resonance
GPU	Graphics processing unit
MM	Metamaterial
PD	Planar diode
PEC	Perfect Electric Conductor
SRR	Split ring resonator
TE	Transverse electric

Preface

Bodies in classical electrodynamics are considered as small scale objects when their dimensions are much smaller than the wavelength they interacting with. Such a description is suitable for a simple form homogeneous object, such as metal or dielectric sphere, cylinder and similar body of general shape. Up-to-date electrodynamic problems solved in practice usually deal with complex objects. They consist of parts having various size and shape, which are made from materials with different electrical properties as well. Moreover, the objects interact with electromagnetic (EM) pulse, that contains a wide range frequency spectra. In such situations the classical small scale body criterion loses its meaning. It should be extended to small object specifics, which appears in the EM problem when at least one important detail in terms of the dimensions are smaller than the largest interesting wavelength in the pulse spectra. Such a criterion is satisfied in most problems that are solved in fields of modern high frequency microwave and terahertz electronics.

The objects of study in this doctoral dissertation are from intensively developing field of the high frequency microwave electronics. Therefore investigated structures, in addition to the above discussed specifics of small objects, are small in respect to the usual scale of the human eye — their dimensions are of microscopic level. For this reason, one encounters certain difficulties on both research stages: modelling and experiment.

All investigation performed in this work is based on research results obtained by computer simulation. Considerable part of them is also confirmed experimentally. For numerical calculations finite-difference time-domain (FDTD) method [1] is used. It allows calculating time dependence of EM field components within modelled region. The main challenge currently facing the modelling of small-scale problems is requirement for large or even huge computational resources, such as computation time or amount of computer memory. It is evident that being interested in the evaluation of EM field

components within a small region in comparison with the wavelength, one has to use small discretization step. This leads to the large amount of nodes in which EM field components are evaluated and in turn results in high computer memory consumption and long processing time in computers central processing unit (CPU). Therefore, the variety of measures were undertaken to speed up the calculations. First of all, the model is simplified. Further, we implemented modifications of the computer model, by including additional calculation methodologies. They enabled the increase of the discretization step size and let us to reduce the number of nodes required for calculation by several hundred times. And finally, we took advantage of parallel computing technologies, which allowed calculating more EM field values during the same period of time. Solving encountered problems we not only received relevant physical results, but also contributed to the development of FDTD method. In addition, the real abilities of using graphics processing units (GPU) and computer clusters for speeding up FDTD calculations were estimated.

Relevance

The rapid development of the terahertz technologies are increasingly faced with complex small objects. Modelling of their electrodynamic properties is very important phase of research, because experimental investigation of various configurations of micron-sized structures is very inefficient due to high cost of fabrication. Nevertheless, huge amount of computing resources are needed for realisation of computer models of electrically small objects. On the one hand, it is essential to develop new numerical techniques which allow reducing the size of numerical problem. On the other hand, it is relevant to examine more powerful computing systems for speeding up the calculations. In the dissertation we contributed to the both of these fields.

Scientific novelty

Equations derived in this work allow implementation of two-dimensional electron gas (2DEG) sheet characterized by specific surface conductivity in a FDTD calculation scheme. They were proved by solving model problem and were also used for modelling of planar arrays of split-ring resonators (SRR).

It was shown that resonant modes of electric current induced in a single

SRR causes band-stop filtering effect in the transmission spectra of planar SRR array. The modes of electrical current in simple symmetric and asymmetric SRR have been determined. The serial current mode occurs in asymmetrical SRR only. The band-stop resonance in transmission spectra caused by this mode has very high resonance quality factor. It promises high application potential in terahertz switching and filtering systems. The influence of Fabry-Perot resonances, arising in dielectric substrate, on transmission characteristics of the planar SRR array was investigated. It was demonstrated that by choosing proper thickness of the substrate one can significantly increase modulation depth of the planar SRR array based modulator.

The performance of semi-automatic parallelization tool ParSol for accelerating FDTD calculations on multiprocessor systems was investigated. Using it a significant calculation speed-up and access to a large amount of computer memory was achieved solving the huge computational problem of a planar diode interaction with TE_{10} electromagnetic wave in a rectangular waveguide. It was shown that behaviour of the planar diode sensitivity qualitatively corresponds to the dependence of the gain of a dipole antenna on frequency. The condition was established that allows keeping smooth sensitivity of the planar diode in different waveguide frequency bands.

Investigation of acceleration of FDTD calculations in computers graphic cards revealed that graphics processing units (GPU) with computing capability 2.0 or higher have automatic on-chip cache memory management that deals with high global memory latency time.

Practical importance

Two-dimensional electron gas (2DEG) layers characterized by very large electron mobility are increasingly used in modern electronics. Proposed method for accounting 2DEG in FDTD procedure lets calculation of the EM field components which are important for the performance of the particular device. The method was also applied for modelling of losses of the EM field in the walls of waveguide resulting from the finite conductivity of metal. In this case skin-depth region was transformed into two-dimensional layer enabling the use of derived surface conductivity FDTD equations. Such transformation allows simplifying the model and reduces the size of numerical problem. This approach was applied to simulate planar arrays of

SRRs as well.

For the planar diode placed in the waveguide it was shown that by choosing proper height of the waveguide, the sensitivity of the diode can be done practically the same for different frequency band waveguides.

The resonant frequencies of current modes in a single symmetric and asymmetric shape resonators were established. This enables prediction of the filtering frequency from the SRR size and dielectric constant of the substrate. High modulation efficiency can be achieved by choosing proper thickness of the substrate and employing the serial current mode in the asymmetrically shaped resonator when modulator is switched either optically or electrically. It is very important for the development of the modulators for terahertz communication and real-time imaging systems.

The GPUs become increasingly important for the accomplishment of numerical simulations. Their computational power and memory amount is growing rapidly. Besides, the power and price ratio of the GPU is much better than of the CPU. This enables the transfer of large scale FDTD calculations to the computer graphics cards. In the nearest future it might be expected to execute more complex and accurate electrodynamic models on the GPU based systems.

Main objectives

1. To derive FDTD equations for modelling of two-dimensional conductive layers, characterized by specific surface conductivity.
2. To speed up FDTD calculations in multiprocessor systems — computer cluster and graphics card — using high level programming tools.
3. To perform the investigation of the planar diode sensitivity characteristics in different frequency band rectangular waveguides, and obtain frequency independent sensitivity in a broad frequency range.
4. To determine the dependence of the resonant properties of the split ring resonator on its size and geometry, and evaluate the possibility to use the planar resonator arrays for development of the active metamaterial in terahertz frequency.

Key statements for defence

1. The layer, characterized by specific surface conductivity, can be accounted for in FDTD method by modifying the calculation of the tangential

electric field components in a two-dimensional conducting layer plane.
2. The frequency independent response of the planar diode can be obtained by choosing suitable waveguide height b for the particular frequency band in such a way that the ratio b/a should be kept constant switching from one waveguide band to the other.
3. Serial mode of electrical current induced in asymmetric split ring resonator results in a high quality factor band-stop resonance in transmission spectra of planar array made from such resonators.
4. By changing the thickness of the dielectric substrate, one can improve modulating properties of planar split-ring resonator array placed on the substrate.

Contribution of the author

The author of this dissertation has developed C++ applications that simulate electrodynamic problems described below. He also contributed to the development of parallel versions of these programs. Using the developed software he performed a number of simulations, analysed the results. He also contributed to the scientific publications and conference presentations which have been made during preparation of this doctoral dissertation.

Layout of the doctoral dissertation

The dissertation consists of the introduction, five chapters, conclusions and bibliography. Short summaries of each chapter are presented below.

1 Theoretical introduction and review of scientific articles related to the dissertation

This chapter consists of four sections. It will introduce the reader to the investigations carried out in this doctoral dissertation and their importance to the specific fields of the microwave and terahertz electronics. It contains the synthesis of the theoretical knowledge required to understand research methods and processes taking place in the targeted objects and the contribution of the author to the development of researched fields in the context of other authors works. In the first section the basis of the FDTD method and additional numerical techniques used in this work are explained. In the second section the parallelization possibilities of the FDTD computational algorithm are discussed. In the next two sections 1.3 and 1.4 the investigated small-scale structures — in particular planar diodes and split-ring resonators are reviewed. In the last section of the chapter the objectives of the doctoral dissertation are formulated.

2 Two-dimensional layer characterized by specific surface conductivity

In this chapter the technique for the implementation of a two-dimensional conducting layer, characterized by specific surface conductivity, in a FDTD scheme is proposed. The modified EM field update equations are derived for the calculation of the tangential electric field components in the layers plane. The reliability of the proposed technique is checked applying it to the

simple problem — the dependence of the electromagnetic wave reflection on the surface conductivity of 2DEG sheet covering completely cross-section of the rectangular waveguide. The obtained results are compared with the available analytical solution. It was shown, that obtained equations can be used for simulation of EM field power loss due to presence of the electrical conductor. As an example, TE_{10} wave propagation in the lossy rectangular waveguide are simulated.

2.1. FDTD equations for 2DEG

Considering surface currents in the two-dimensional conducting sheet we have to modify a single Maxwell equation, namely, the Ampere's law, rewriting it as follows:

$$\frac{\partial \mathbf{E}}{\partial t} = \frac{1}{\varepsilon}\left[\mathrm{rot}\mathbf{H} - \gamma_s \delta(z - z_k)\mathbf{E}_{\|}\right]. \tag{1}$$

Here $\mathbf{E}$ is the strength of electric field, $\mathbf{E}_{\|}$ — the electric field components tangential to the sheet plane, $\mathbf{H}$ is the strength of magnetic field, and $\gamma_S = Z_0\sigma_S$ is normalized specific surface conductivity of the layer. The symbol $\delta(z)$ stands for the Dirac function. Coordinate and time variables in this equation are normalized.

Compared to the standard expressions for calculation of tangential electric field components in lossy materials the only difference is that bulk conductivity γ in 2DEG case is replaced with $\gamma_S/\Delta z$, where Δz stand for the discretization step along the normal to the sheet coordinate axis. Tangential electric field components outside the sheet and all other components of the electromagnetic field has to be calculated by means of the standard update equations.

2.2. 2DEG sheet placed within rectangular waveguide

In order to illustrate the efficiency of the proposed method we modelled the propagation of TE_{10} electromagnetic wave along the rectangular waveguide which is divided into two parts by the 2DEG sheet. Due to the simple geometry this problem enables to obtain the analytic solution based on the matching the incident, reflected and transmitted waves at the interface. We used the analytic result to estimate the accuracy of the numerical simulation.

The dependencies of the absolute value of the reflection coefficient R on the

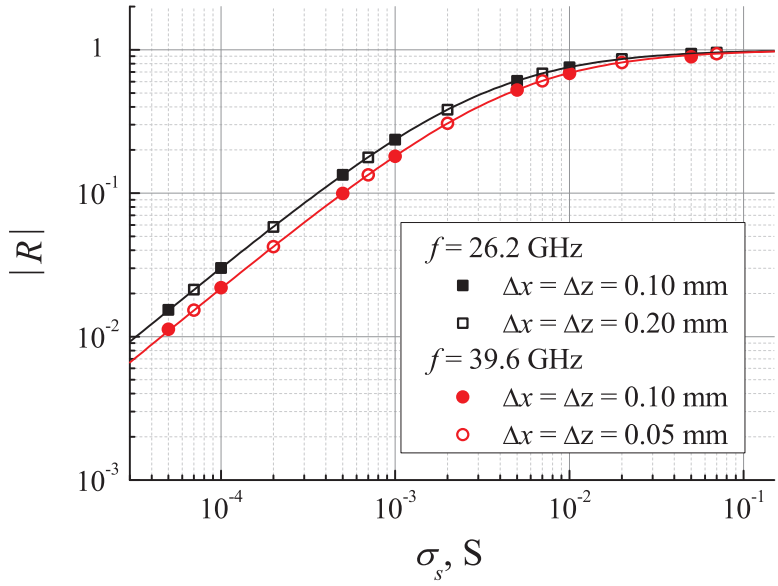

Figure 1: Dependence of the absolute value of the reflection coefficient on 2DEG sheet's surface conductivity. Points correspond to the FDTD modelling, solid lines show the analytical solution. $a = 7.2$ mm.

specific surface conductivity are shown in Fig. 1 for two different frequencies and Δz values. As one can see from the figure, the points of reflection coefficient obtained numerically fits well solid lines corresponding the analytical solutions. It is seen that in the considered step size range the result is independent of Δz though it appears in the approximation of the 2DEG conductivity. It should be pointed out that the electric field near the 2DEG sheet in this particular case depends only on reflection coefficient R, so a high precision of R automatically leads to the precise values of the electromagnetic field components in the whole model. Therefore results presented in Fig. 1 validates the reliability of proposed modification to the FDTD update equations in 2DEG area.

2.3. Simulation of EM field power loss in electrical conductor using FDTD method

It can be shown that two-dimensional conducting layer absorbs the same amount of EM field power as the bulk conductor with specific conductivity σ, when its specific surface conductivity is equal to:

$$\sigma_S = \sqrt{\frac{\sigma}{2\omega\mu_0}} = \delta\sigma. \tag{2}$$

Here ω is angular frequency of the EM wave, μ_0 is vacuum permeability, and δ is the skin-depth in conductor.

So, in order to calculate layers surface conductivity, which will result in the same absorption of EM power as the bulk metal surface, metals specific conductivity σ should be multiplied by the skin-depth in particular frequency. We applied this technique for modelling loss of TE_{10} wave propagating through the section of empty rectangular waveguide. The waveguide walls are made from the metal with finite conductivity, that is why propagating EM wave is slightly absorbed.

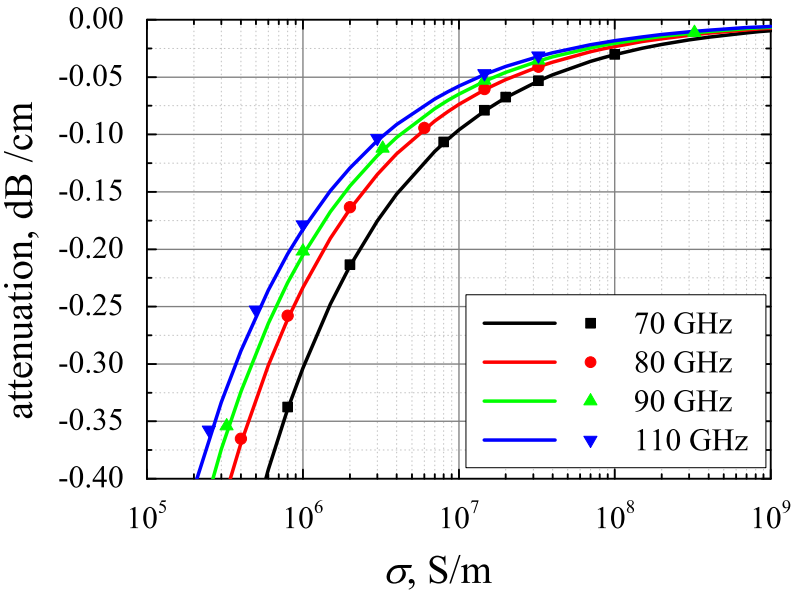

Figure 2: Dependence of TE_{10} wave attenuation on specific conductivity of the rectangular WR-10 waveguide walls. Different shape of the dots correspond to the different frequency of the modelled wave, solid lines — analytical solution. $a = 2.54$ mm, $b = 1.27$ mm.

For the simulation WR-10 waveguide was chosen because it is designed to operate in high frequency range, where power loss is higher, so smaller section of the waveguide should be modelled to evaluate the attenuation coefficient. The waveguides made from different specific conductivity materials were modelled at different wave frequencies. The attenuation was calculated from the decrease of the electric field amplitude in the centre of the waveguide. The results presented in Fig. 2 indicate good agreement between FDTD simulation and theory [2]. This confirms that using skin-effect

approximation one can transform bulk conductor into two-dimensional layer which can be included in the FDTD calculations using expressions provided in this dissertation. This allows to simplify the numerical model and significantly reduce the amount of calculations. It should be noted that such a approximation has limitation — the attenuation is accurately evaluated for one particular wave frequency value only.

3 Parallelization tools for accelerating FDTD algorithm

In this chapter the parallelization techniques for FDTD algorithm is considered. They allow to exploit computational capabilities of multiprocessing systems for acceleration of FDTD calculations. Although these parallelization techniques can be relatively simply numerically implemented, they still remain highly efficient. The parallelization of the FDTD algorithm is based on the domain decomposition method. The tool of parallel linear algebra objects ParSol [3] is used to get a semi-automatic implementation of parallel algorithm on distributed memory computers. Some results of numerical simulations are presented and the efficiency of the proposed parallel algorithm is investigated. Parallel numerical algorithms to solve the 3D mathematical model on GPU are considered. Results of numerical tests performed on different GPUs are presented.

3.1. FDTD calculations in computer cluster

The parallel version of FDTD algorithm is generated semi-automatically by using the tool of parallel linear algebra objects ParSol. ParSol is C++ programming library, written by Alexandr Jakušev [4] during PhD studies in Vilnius Gediminas Technical University. The parallelization is based on the domain decomposition method, when discrete grid is divided into the subvolumes and they are distributed among all processors of the computational system.

Computational experiments were performed on "Vilkas" cluster of computers at Vilnius Gediminas Technical University. It consists of nodes with

Table 3.1: Results of computational experiments on "Vilkas" cluster

$n \times m$	2×1	1×2	4×1	2×2	1×4	8×1	4×2	16×1	8×2
S_p	1.98	1.63	3.27	3.11	1.65	6.14	5.59	11.84	10.80
E_p	0.99	0.82	0.82	0.79	0.42	0.77	0.70	0.74	0.68

Intel Core2 Quad processor Q6600. Obtained performance results are presented in Table 3.1. Here for each number of processors n and active cores within processor m the coefficients of the algorithmic speed up $S_p = T_1/T_p$ and efficiency $E_p = S_p/p$ are presented. Here p is total number of active cores. The grid size of the discrete problem is $(261 \times 101 \times 569)$. The presented results confirm the conclusions of the standard scaling analysis of the parallel domain decomposition algorithm. In the case when up to two cores per node are used, the efficiency is high and decreases slightly when number of processors is increased. It can be recommended to use till two cores per one node in practical simulations. In the case of four cores per node data reading/writing operations start to be a bottle-neck of the parallel algorithm, since the discrete scheme is defined on a very sparse stencil and no intensive local computations are needed to update the solution at each grid point.

Only by using ParSol library and computer cluster "Vilkas" we were able to solve very large numerical problem of planar diode interaction with TE_{10} wave propagating through the rectangular waveguide.

3.2. FDTD calculations in computers graphic card

Being an integral part of a modern computer, a GPU is performing a huge number of floating point operations per second. GPU consists of array of streaming multiprocessors (SMs). They actually perform calculations executing blocks of threads. In general a new GPU overcome any new CPU in terms of performance/price ratio. However, GPUs have many restrictions and require specific algorithms to accomplish these restrictions and to use GPUs resources efficiently. The most important task of efficient calculations on GPU is the implementation of the optimal data transfers among different layers of memory. That is why the main indicator of the GPU computation efficiency is bandwidth. The bandwidth obtained by application compared to its theoretical value shows how effectively GPU is used.

The GPU memory is divided into the following hierarchy: (a) host memory, which is not actually a part of the GPU, therefore the device must transfer data from/to host; (b) global memory, which is accessible by all threads that run on all SMs; (c) shared memory, which is located on each SM and is accessible only to the threads of the same block. The shared memory is much faster than the global memory, but it has a very limited size.
The problem should be split into blocks of SIMD (Single Instruction Multiple Data) tasks, which are performed by different threads in parallel. Array of blocks is constructed, and each block is indexed by using one-, two- or three-dimensional indexing. Tasks in a block are assigned to the threads, which are indexed inside the given block.
Since the shared memory of the device has a very limited size, the sizes of blocks defining subtasks should be small enough. We investigated whether the usage of shared memory can help to optimize the efficiency of the calculations. GPUs of compute capability 2.x support data L1 caching technology. Physically it uses the same on-chip memory as shared, but in contrast to latter it is handled automatically. Comparing the efficiencies of both realizations is a goal of our investigation.

Table 3.2: The calculation time in different GPUs and CPU

	GeForce® GTX 460	GeForce® GTX 650 Ti	CPU
shared memory	177 ms	324 ms	1060 ms
L1 cache	179 ms	214 ms	
bandwidth	128 GB/s	86.4 GB/s	21 GB/s

We performed several numerical tests using computational scheme which solves three-dimensional EM problem that describes a wave propagation in a rectangular waveguide. In Table 3.2 software realizations with shared memory and L1 cache are compared in respect of CPU (Intel® Core™ i7 2600) usage. It is seen that the calculation time when using L1 automatic data caching is similar to the case when data is transferred to the shared memory. For GPU GeForce® GTX 650 Ti calculation time using L1 cache is even shorter than using shared memory, but is still slightly longer than for GPU GeForce® GTX 460. This could be explained by significantly lower theoretical bandwidth peak of GTX 650 Ti. The results of the tests confirm that L1 automatic caching technology can successfully replace shared

memory in FDTD calculations using GPUs with 2.0 or higher compute capability. This extremely facilitates the programming, since there is no need to carry out low-level memory management procedures.

4 Interaction of the planar diode with TE_{10} wave propagating through rectangular waveguide

In this chapter numerical investigation of a thin asymmetrically shaped planar diode (PD), which is in fact a microwave detector operating over a broad frequency range, was performed. The PD is inserted in the centre of a rectangular waveguide with propagating TE_{10} wave. In the first section, PD model used in simulations is described. In the second section, investigations of the electric field distribution within the mesa and the reflection coefficient from the PD are presented. In the third section, the sensitivity of the PD is considered and the optimization of the diode frequency response is presented.

4.1. Numerical model of planar diode

To build the numerical model of the PD we have used the characteristics of the detector presented in [5]. The PD is in general a multi-layered structure grown on a semi-insulating substrate. Because of the limitation of the sub-cell technique we have used in calculations, we were able to take into account only one of the layers — the layer that makes the greatest influence in the interaction of the diode with EM wave. Therefore, the model of the investigated structure consists of a thin doped GaAs layer (mesa), inserted between two metallic contacts covering its ends. In order to calculate electric field strength in the mesa and reflection coefficient from the PD, the waveguide section with PD was modelled. It was placed in the center of the waveguide at the one wavelength ahead from the wave excitation plane and at the same distance before the end of the modelled section. TE_{10} wave in the waveguide was excited by the current source placed at some

distance from the beginning of the waveguide section. Reflection coefficient was determined from the amplitudes of the partly standing wave appearing between current source and PD. On the ends of the modelled waveguide section non-reflecting boundary conditions was set.

Since the thickness of the active GaAs layer is much less than the wavelength of the EM wave, direct account of it in the FDTD calculation procedure needs a very fine grid. Due to complicated geometrical shape of the mesa, the fine grid in the transverse direction is also desirable. To reduce the number of calculation nodes in longitudinal direction, we have used the sub-cell method proposed by Maloney and Smith [6]. This approach allows to use the space step size that is much larger than the thickness of the layer. Even though using this approach, each EM field component should be calculated at more than 10^9 space points, at each time step. For this reason the parallel version of the FDTD algorithm was developed, using ParSol data parallelization library [3]. The calculations were carried out on computer cluster "Vilkas" at Vilnius Gediminas Technical University. Furthermore, to improve the description of mesas geometry in the discrete FDTD grid, we have used volumetric approach where the permittivity and conductivity of the single FDTD cell are set proportional to the volume that mesa fills in the current cell.

4.2. Electric field within PD mesa

We calculated the distribution of the electric field amplitude in the mesa by interacting with TE_{10} wave. Two different shape mesas: V-shaped mesa of PD (Fig. 3a) and necked mesa of bigradient diode (Fig. 3b) were investigated. Our preliminary calculations have revealed that the E_y component of the electric field plays the leading role in the mesa. So we have focused on the analysis of the distribution of E_y component along y coordinate, averaged in x direction within mesa.

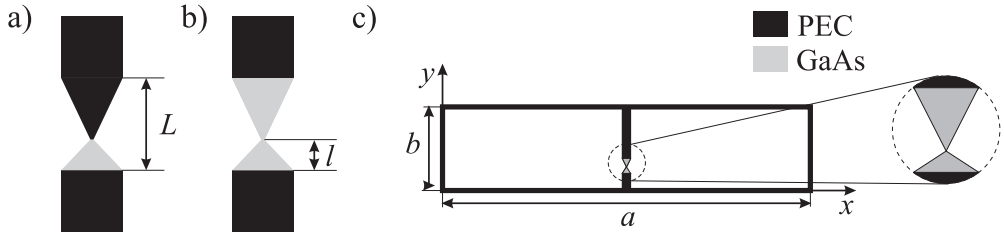

Figure 3: a) Planar diode; b) Bigradient diode; c) Front view of the PD in rectangular waveguide.

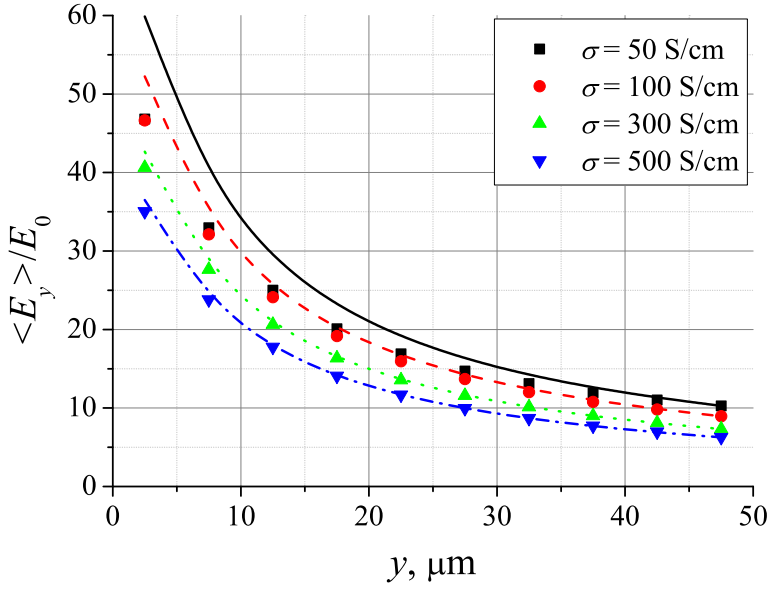

Figure 4: Averaged in x direction electric field dependence on coordinate y for different specific conductivity PD mesa's. Dots correspond to the FDTD calculation results, solid line is drawn according to approximation (3). Calculation parameters: $f_{\mathrm{Ka}} = 33.4$ GHz, $L = 50$ μm.

FDTD calculation results of the averaged electric field distribution within different specific conductivities PD mesas (Fig. 3a) are shown in Fig. 4 by points. One can see that with the increase of specific conductivity the electric field amplitude decreases. The largest electric field always appears at the necked part of the mesa. It is seen that the ratio between maximum and minimum amplitude values increases with the growth of specific conductivity. Let us assume that DC voltage is applied to the mesa. Supposing that the drift velocity of electrons in GaAs is independent of the electric field strength, one can calculate the dependence of electric field in the mesa by solving Poisson equation [7]

$$\langle E_y \rangle (y) = \langle E_y \rangle_0 \frac{w_0}{w(y)}. \tag{3}$$

Here $\langle E_y \rangle_0$ is the electric field amplitude on a broad GaAs-metal interface, where the width of PD is w_0 and $w(y)$ denotes coordinate dependent width of the PD. Calculated according to (3) dependences of electric field strength in the mesa on coordinate are shown in Fig. 4 by solid lines.

It is seen that this simple approximation fits well with the FDTD calculation results until conductivity of the mesa is sufficiently high and conduction current dominates in it over the displacement current. This fact is also

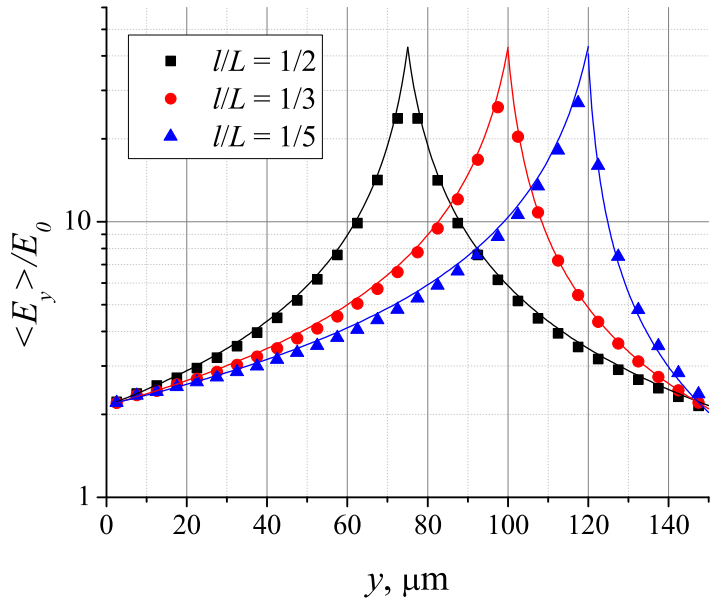

Figure 5: Averaged in x direction electric field dependence on y coordinate in a bigradient diode mesa for different ratios l/L (ref. Fig. 3b). Dots correspond to the FDTD calculation results, solid lines show approximation (3). Calculation parameters: $\sigma = 500$ S/cm, $f_{\mathrm{Ka}} = 33.4$ GHz, $L = 150$ μm.

confirmed by the electric field amplitude distributions within the different shape bigradient diode mesas, shown in Fig. 5. The values calculated using FDTD method are indicated by points, the solid lines are drawn according to formula (3).

The specific conductivity of PD mesa investigated in [5] is 1.25 S/cm. This is much lower than the value that is needed for (3) approximation to be valid. In such a case the gradient of the electric field amplitude in a bigradient diode is quite small, because electric field concentrates on the GaAs-metal interfaces, in contrast to the PD mesa, where the amplitude reaches its maximum value at the neck of the mesa, even when its specific conductivity is relatively low. The electric field in the necked-part of the PD mesa remains large due to the influence of metal concentrator. This is the basic difference between the bigradient and planar diodes. The latter ensures non-homogeneous electron heating even in a low conductivity mesa.

Considering the amplitudes of the other components of the electric field near PD it should be pointed out that due to symmetry of the layer E_x component in the symmetry plane is zero and slightly increases moving

away from it. The amplitude of E_z is negligible, so the component E_y dominates within the mesa.

4.3. Optimization of PD voltage sensitivity

PD can be considered as planar analogue of a point-contact diode. The asymmetrical shape of mesa causes the non-uniform distribution of electric field in it and consequently leads to the non-uniform electron heating in the structure when it interacts with microwaves. As a result, a DC voltage appears on the ends of the structure [7] enabling microwave power measurement. Since electron heating effect is put on a basis of the proposed device performance, it can be used in a wide frequency range up to a terahertz region [8], where a traditional semiconductor diode based on microwave current rectification is of a little use. Experimental results indicate that voltage sensitivity of planar diode is nearly independent of frequency in range from 10 GHz to 0.8 THz [9]. This is a very interesting fact because experiments have been performed covering several waveguide frequency bands and using different dimension waveguides [5]. It should be noted that the electric field strength in the empty waveguide at constant electromagnetic wave power strongly depends on two factors: dimensions of the waveguide and the frequency of the wave. On the one hand, as dimensions of the waveguide become smaller, the electric field should be larger to transfer the same power through the waveguide. On the other hand, for the fixed size of the waveguide window the electric field strength in the empty waveguide E_0 decreases with the frequency due to dispersion of the electromagnetic wave.

To calculate the frequency response of the detector, we have used voltage sensitivity S expression derived using warm electron approximation [8]:

$$S = \frac{\mu_0 \left((w/d)^2 - 1\right)}{12 \ln\left((w/d) + 1\right)} \frac{\left\langle E_y^2 \right\rangle}{P_i} N. \tag{4}$$

Here μ_0 refers to a low-field electron mobility, which can be expressed through specific resistance ρ and electron concentration in the mesa region, which are also listed in [5]. E_y is a electric field within the mesa, which is determined from the FDTD simulation, P_i stands for the power of an incident wave, h denotes the thickness of the device and d refers to the width of the necked-part of the mesa. The multiplier N has the dimension

of time and accounts for the influence of different relaxation times on the sensitivity. It is worth to mention that within the considered frequency range 20–140 GHz N is practically independent of frequency [5] and can be expressed as

$$N = \tau_M + (1 + s)\tau_\mathcal{E}, \tag{5}$$

where τ_M stands for Maxwell relaxation time, $\tau_\mathcal{E}$ is an electron energy relaxation time and s is the exponent in the dependence of the electron momentum relaxation time on energy. The parameters characterizing investigated PD are collected in [5]: $\rho = 1.25$ S/cm, $w = 100$ μm, $d = 12$ μm, $\tau_M = 910$ fs, $\tau_\mathcal{E} = 450$ fs ir $s = 1$.

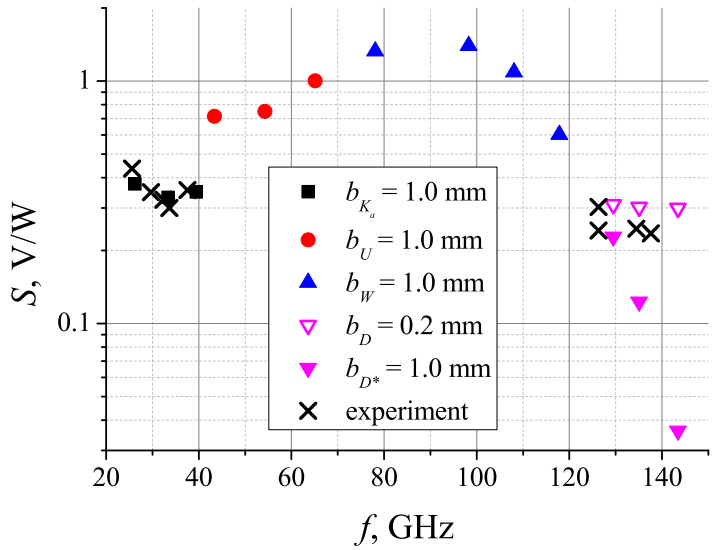

Figure 6: Dependence of the PD sensitivity on microwave frequency. Points correspond to the modelling, crosses show experimental results.

By calculating the average electric field in the mesa, the sensitivity of the PD can be determined. Results of our calculations are shown in Fig. 6 by points. Different shape of the points indicates different frequency bands. Dimension of short waveguide wall b is presented in the legend of Fig. 6, where b index denotes the frequency band. As one can see, waveguides used in experiments are narrowed, because the dimension of the shortest wall b is smaller than the standard. It should be pointed out that calculated results fairly well agrees with the results from the experimental measurements and this confirms the model used as reliable.

Considering calculated results in D band for $b = 0.2$ mm and 1 mm, it is seen that the height of the waveguide window strongly influences the sensitivity of the planar diode. This fact gives an idea to use the size of the window b as a parameter adjusting the sensitivity of the PD at particular frequency band. When b is set 0.2 mm in D band (open triangles in Fig. 6) the sensitivity values is almost independent of frequency. Moreover, the decrease of b leads to the essential decrease of the reflection coefficient from PD. Decreasing b we could improve both main PD characteristics: getting the frequency independent response of the diode and keeping the reflection coefficient at sufficiently low level that is acceptable for power measuring device.

Calculated dependences of the average electric field in the mesa on a ratio b/a in different frequency bands revealed that $\langle E_y \rangle$ is proportional to the $\sqrt{b/a}$. Additional calculations performed only for the metal contacts without the mesa showed that contacts by themselves govern almost all reflection from the structure and establish roughly the same electric field distribution between them as it is in the structure with the mesa. Since metal contacts play so essential role in the PD performance, one can assume that the structure under consideration acts as a small dipole antenna placed in the center of the waveguide. Consequently the voltage drop induced across the mesa by the microwave electric field should be proportional to the total length of the structure b multiplied by the strength of the electric field E_0 in the center of the empty waveguide. Since E_0 depends on the size of the waveguide window as $E_0 \sim 1/\sqrt{ab}$, one can readily get

$$\langle E \rangle \sim bE_0 \sim \sqrt{\frac{b}{a}}. \tag{6}$$

It is worth to mentioning that behaviour of the PD sensitivity calculated for $b = 1$ mm (ref. to Fig. 6) qualitatively corresponds to the dependence of the gain of a dipole antenna on frequency: the gain is independent of frequency in a low frequency limit, later it grows on with frequency, reaches its maximum, and sharply decreases in a high frequency limit.

Since PD sensitivity depends on the averaged electric field amplitude in mesa (4), by keeping ratio b/a constant one can obtain flat frequency response. Having in mind that reflection coefficient value should not exceed 0.1 the ratio b/a should be chosen less than 0.15.

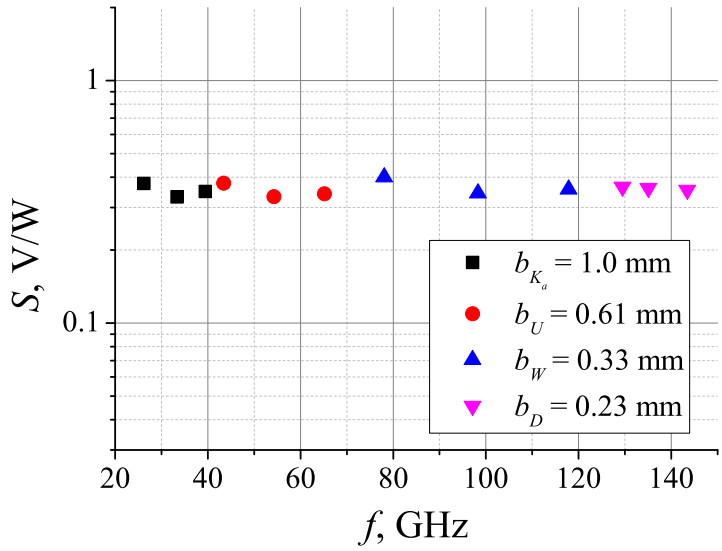

Figure 7: Dependence of the optimized planar diode sensitivity on microwave frequency, when $b/a = 0.139$.

Performing optimization of frequency response of the PD the ratio $b/a = 0.139$ was chosen. Calculated results of the sensitivity are shown in Fig. 7. Corresponding sizes of b are presented in the legend of the figure. As one can see, the sensitivity of the diode is between 0.32–0.40 V/W over frequency range from 26 to 143 GHz. It is worth to mention that the other ratio b/a can be chosen for optimization depending on the desirable sensitivity and reflection coefficient.

5 Tuning of resonance frequency in array of split-ring resonators in terahertz region

In this chapter the investigation of planar arrays of split-ring resonators (SRR) formed on semiconductor plate is presented. Our aim was to investigate the resonance properties of SRR array and demonstrate the possibility to effectively tune the SRR resonance in terahertz region. In the first section, different types of resonant current modes in a single SRR are considered. In the second section, the relevance between the band-stop filtering

effect in pulse transmission spectra and the current resonances within single SRR is identified. The dependence of the resonant frequency on the size of the SRR is established. In the third section, tuning of the band-stop frequency of SRR array is demonstrated in two different ways: by optically changing the resonant current mode and by changing the depletion capacitance of the integrated Schottky barriers. In the fourth section, influence of Fabry-Perot resonance (FPR) appearing in the semiconductor plate on SRR resonance is considered. It was found that modulation properties of SRR array strongly correlates with the thickness of the plate. The conditions for the maximal pulse power modulation were determined.

5.1. Resonant modes of electric current in SRR loop

SRR is made from high conductivity metal stripes. In the individual SRR model, we assumed that the stripes are perfectly conductive, so the tangential electric field components within the stripe becomes zero. A differentiated Gaussian pulse is applied as the current source to excite wide spectra (to 1.6 THz) plane wave, propagating away from the excitation plane. The time dependence of the electric current induced in the stripes was calculated according to Ampere's Law [1]. Applying Fourier transform the frequency spectrum was obtained.

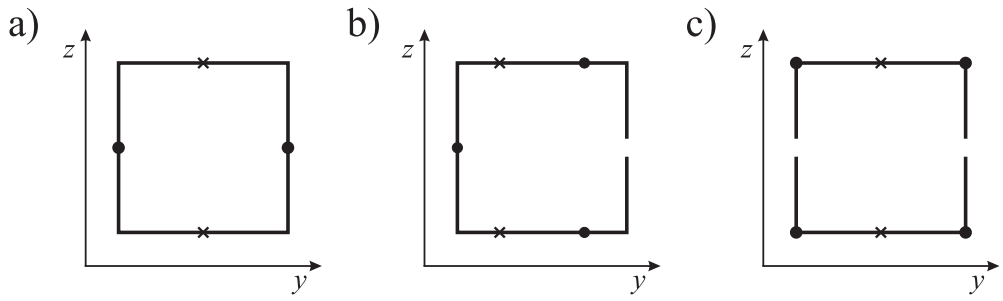

Figure 8: Resonators under investigation: a) closed ring; b) asymmetric SRR; c) symmetric SRR. Points indicate maximum current amplitude positions, crosses — minimum amplitude positions.

To find out how the SRR interacts with EM pulse we investigated different types of resonators (Fig. 8): a) closed ring; b) asymmetric SRR; c) symmetric SRR. The polarization of the EM wave is chosen so that the electric current in the structures is excited by the electric field only. Because the electric field of the excitation pulse is of the same direction in both collateral stripes, the direction of the current in respect of the loop of the resonator

is opposite. In the symmetrical structures (a) and (c) in Fig. 8, the current does not flow in the central points of the horizontal stripes. It can be explained by the symmetry of the resonators in respect of the field.

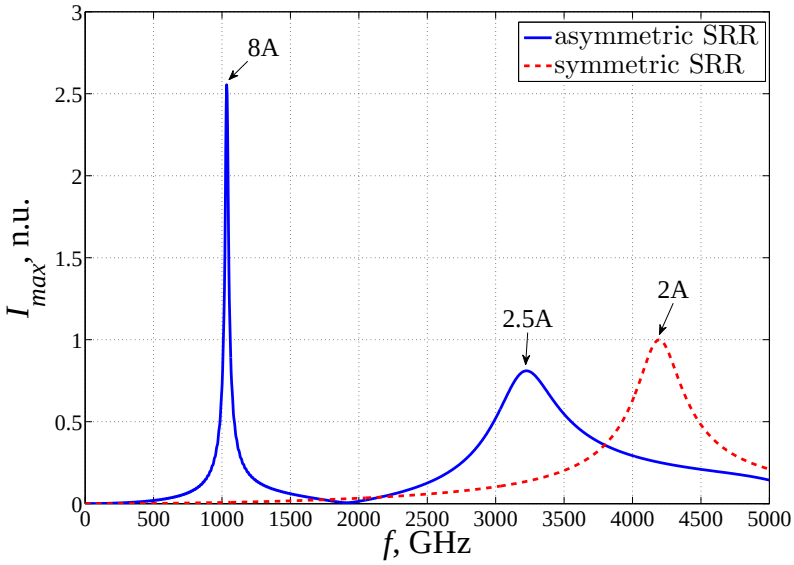

Figure 9: The spectra of the current at the maximum amplitude position in the symmetric and asymmetric SRRs normalized to the peak value of symmetric SRR spectra. Arrows indicate the effective wavelength of particular resonance frequency, where A is a side length of the resonator.

Two current modes in the SRR were found, appearing as resonances in the current spectrum: 1) parallel mode — corresponding to the currents in the vertical stripes of SRR flowing in the same direction; 2) serial mode — corresponding to the currents in the vertical stripes flowing in the opposite directions. The parallel mode is observed in both symmetric and asymmetric structures (Fig. 9). This mode is induced by the external electric field and vanishes quickly (within 2 ps) after the excitation pulse passes the SRR. The serial mode occurs only in the asymmetrical SRR. As the parallel mode disappears, the current begins to flow as in a usual LC circuit, where the ring acts as the inductor and the gap acts as a capacitor. Although the amplitude of the serial current is much smaller than that of the parallel one, due to its small damping, the significant contribution of the serial oscillations is seen in the spectrum. The wavelength of oscillation frequency of the current can be related to the SRR side length A as shown in Fig. 8 with arrows.

Table 5.1: Current resonance frequency relation with the size of the SRR

	f_{serial}	$f_{parallel}$
asymmetric SRR	$\frac{c}{2.5A\sqrt{\varepsilon^*}}$	$\frac{c}{8A\sqrt{\varepsilon^*}}$
symmetric SRR	$\frac{c}{2A\sqrt{\varepsilon^*}}$	—

5.2. Band-stop filtering properties of planar SRR array

For practical applications SRRs are arranged into planar arrays formed on a surface of a solid dielectric substrate. Investigation revealed that the current modes in the loop of a single SRR are strongly associated with the band-stop resonances in the pulse transmission spectra through the array of such SRRs.

More accurate model was used for calculations of SRR array transmission spectra, when SRRs are deposited on GaAs substrate in a plane normal to the x-axis (Fig. 8), forming a regular lattice. SRRs made from gold were considered. Whereas the stripes are very thin, hundreds of nanometres, they were included into modelling as two–dimensional conductive sheets, using technique described in section 2.3. For the modelling of the periodic array we have used the unit cell approach, therefore the only SRR has been modelled with periodic boundary conditions at the edges of the unit cell.

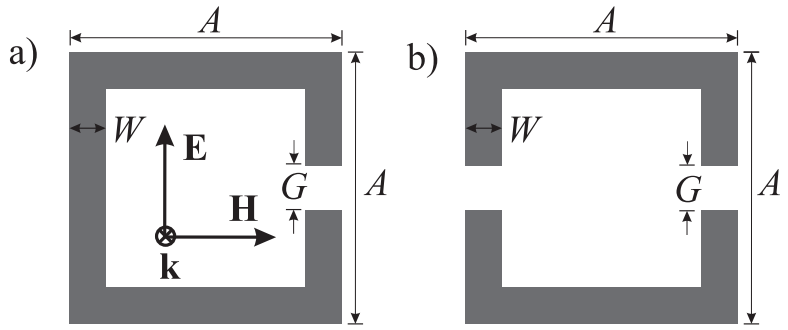

Figure 10: Model of finite conductance SRR: a) asymmetric SRR; b) symmetric SRR.

The asymmetric SRRs (Fig. 10a) as well as symmetric SRRs (Fig. 10b) placed periodically on dielectric substrate show good filtering features at the resonance frequency. The band-stop resonance frequencies of investigated asymmetric and symmetric SRRs in respect of SRR size A are listed in the Table 5.1.

In the table c denotes a speed of light in vacuum, ε^* is the effective dielectric

constant of the substrate, expressed as follows:

$$\varepsilon^* = \frac{\varepsilon + 1}{2}. \tag{7}$$

In general, the frequency and amplitude of the resonance depends on the unit cell size and other SRR dimensions as well, however, Table 5.1 is valid when G and W are small compared to A.

5.3. Tuning of SRR resonance frequency

Results presented in the previous section confirm that resonant current modes flowing within SRR loops filter energy of incident EM field at resonant frequencies, forming band-stop resonances in transmission spectra. It is obvious that by changin the current flow in the SRR loop, its resonant frequency is changed, consequently changing the filtered frequency of the array as well. Optical generation of free carriers in a particular region of substrate is one of straightforward ways to change current flowing conditions in the SRR. We have modelled the change of the specific surface resistance of InGaAs, filling one of the gaps of symmetric SRR (Fig. 10b), from 1000 Ω to 10 Ω. Modelling results indicate that SRR resonance at 250 GHz appears when resistance is decreased because the SRRs are transformed from the symmetric to the asymmetric structures, enabling the change of the power level passed through the SRR array at 250 GHz about 76 %

Integration of controllable micro-circuit elements, such as capacitors [10] or inductors in the SRR is the other way to change the current flow in it. The symmetric SRR, presented in Fig. 10b, may be loaded with varactor diode for the resonant frequency tuning. Due to small dimensions of the SRRs at terahertz frequency their loading with discrete varactors is not directly applicable. Therefore, we consider varactor diodes as integrated mesa structures fabricated on GaAs substrate. We modelled a Schottky barrier varactor fabricated under the stripe close to the one of the gaps of the symmetric SRR. The Schottky contact area is 4×4 μm^2. We assume that the cut–off frequency of the varactor is much higher than 300 GHz [11] and its depletion capacitance can be reduced with external reverse bias from 1.0 down to 0.25 fF/μm^2 [12].

An additional capacitance added to the symmetric SRR force it to become asymmetric. This is confirmed by calculation results shown in Fig. 11, where low frequency parallel resonance is clearly seen (ref. to Table 5.1).

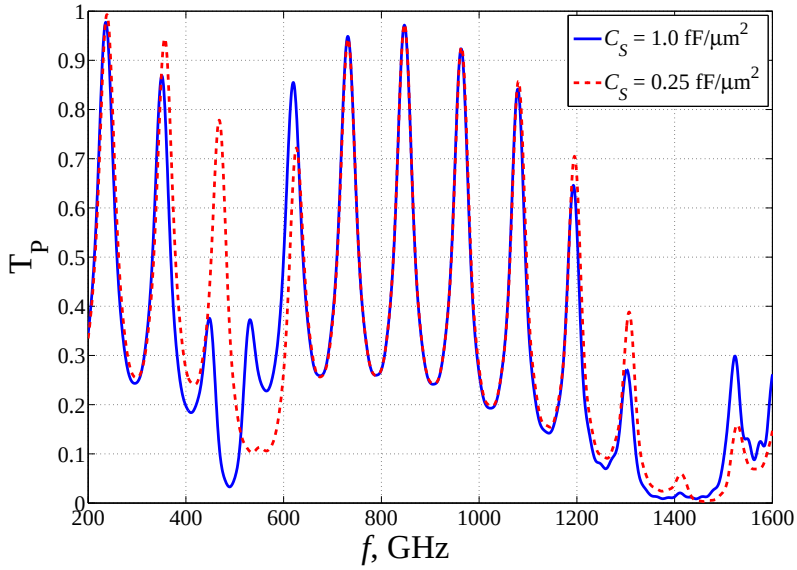

Figure 11: Transmission spectra of the varactor-loaded symmetric SRR with different depletion capacitance of Schottky barrier. Calculation parameters: $A = 36$ μm, $W = 4$ μm, $G = 2$ μm, modelled cell size 50×50; μm^2, thickness of GaAs substrate 350 μm.

It is caused by the serial current mode that appears in asymmetric SRR only. One can see that by decreasing varactors capacitance the resonance frequency shifts to the higher frequency by 13 % and the amplitude of the transmitted signal changes roughly 33 %. It should be noted that SRR band-stop resonance interferes with pattern of FPR, which occurs due to multiple pulse reflections in GaAs substrate. The difference between two curves in Fig. 11 determines the modulation depth at the particular frequency. Due to FPR oscillations it gets the largest value not necessarily at the SRR resonance location at 489 GHz, when $C_s = 1$ fF/μm^2. It is seen that 468 GHz is more preferable; modulation depth at this frequency reaches 66 %.

5.4. Influence of FPR on modulation depth of SRR array

Changing plate's thickness one can shift FPR maximum to desired frequency. Thickening of the plate shifts FPR to lover, whereas thinning it FPR shifts to the higher frequency. By tuning FPR peaks, the transmitted power at particular frequency can be increased significantly, enabling optimization of modulators efficiency. Therefore we calculated the transmission spectra like in Fig. 11 for different thickness of GaAs plate. From these

results the difference of transmitted power ΔP at 489 GHz for two limiting capacitances of Schottky barriers are determined. The dependence of ΔP normalised to incident power P_0 on thickness of GaAs plate is shown in Fig. 12. As one can see the dependence is periodic. Moreover, its period coincides with the period of FPR. The results indicate that GaAs thickness has crucial influence to the modulation depth. The thickness, where the modulation depth reaches maximal values, can be calculated using following formula:

$$T_{diel} = \frac{c\,(n + 0.812)}{2\sqrt{\varepsilon} f}, \tag{8}$$

where n is integer number counted from zero, indicating order of FPR.

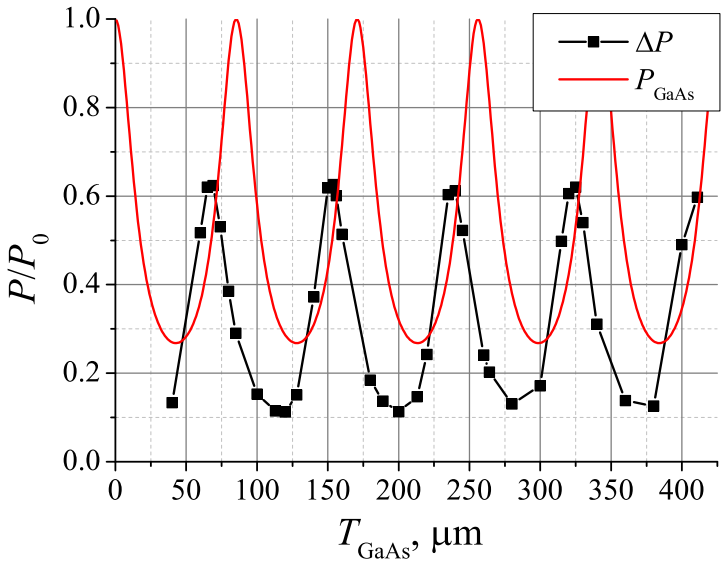

Figure 12: Dependence of normalized modulated power on GaAs plate thickness at 489 GHz is shown by line with dots. Line with dots show calculation results for investigated structures, solid line indicates transmission level of an empty GaAs plate.

To prove that the substrate thickness has real impact on ΔP experimental investigations should be performed. The main difficulty is to manufacture the SRRs with integrated varactors, because it requires complex technological solutions. Therefore, in the initial stage of the research, we designed three different structures shown in Fig. 13, with different geometrical capacitances, simulating different states of the varactor capacitance. The structures with high (a), intermediate (b) and low (c) capacitances are formed on

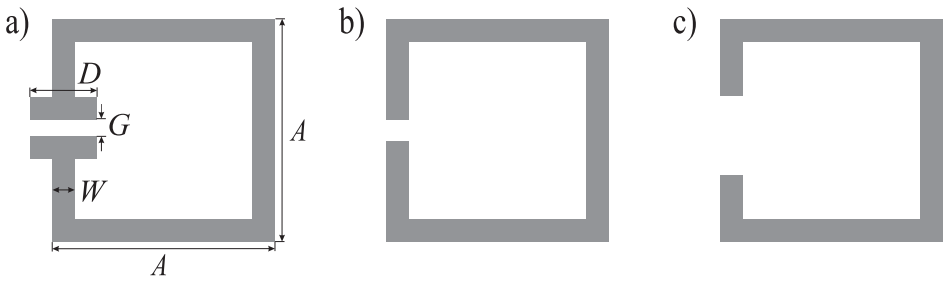

Figure 13: Asymmetric SRR with different gap capacitance. Parameters of SRR: $A = 40$ μm, $W = 4$ μm; (a) $G = 3$ μm, $D = 12$ μm; (b) $G = 3$ μm, $D = 4$ μm; (c) $G = 10$ μm, $D = 4$ μm.

three separate GaAs plates. The transmission spectra are measured using time domain terahertz spectroscopy. Then the samples were thinned and measurements were repeated to obtain the dependence of the transmission on GaAs thickness.

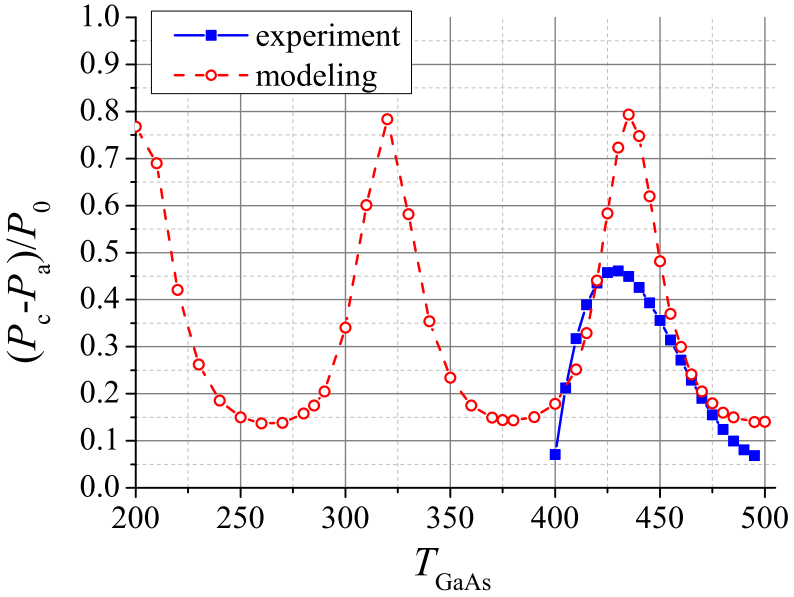

Figure 14: Dependence of normalized transmitted power difference between high and low capacitance structures (ref. to Fig. 13a and 13c) on the thickness of GaAs plate at 360 GHz. Squares show experimental results, open circles correspond to the modelling.

Experimental results together with modelling data are shown in Fig. 14. It is seen that modelling predicts larger modulation depth as measured experimentally. Nevertheless both curves demonstrate similar shape. Calculated optimal thickness according to (8) should be 440 μm that is close to the

values obtained numerically and experimentally. This experimental investigation confirms that modulation depth can be optimized by choosing proper thickness of the dielectric substrate.

6 Main results and conclusions

1. The FDTD simulation of 2D conducting layer, characterized by specific surface conductivity, can be performed modifying the calculation of tangential electric field components within the layer plane. This can be done by replacing specific conductivity in the standard FDTD equations by a specific surface conductivity divided by the normal to the layer discretization step size.
2. Using methods and objects implemented in the C++ library ParSol, the FDTD calculations can be easily and efficiently parallelized in the computer cluster or computer with multi-core CPU.
3. Using the basic functionality of CUDA C programming language without management of shared memory when performing FDTD calculations on GPU with compute capability 2.0 or higher one can speed up the calculations several times in comparison with CPU.
4. Planar diode placed in rectangular waveguide behaves like a dipole antenna and its sensitivity strongly depends on the waveguide height b ratio to the waveguide width a.
5. By choosing proper ratio b/a one can get practically independent frequency response of the planar diode mounted in different band waveguides. Wishing the reflection coefficient from the diode to be less than 0.1, b/a should not exceed 0.15.
6. Serial current mode induced in asymmetric split-ring resonator results in a high quality factor low-frequency band-stop resonance in the transmission spectra of the planar array of SRR. Tuning the frequency or amplitude of this resonance could help to design an effective modulator in terahertz region.
7. By integrating the Schottky barrier diode, acting as a high-frequency varactor, into the gap of split-ring resonator, one can effectively change the

position of high quality factor serial mode resonance.
8. The modulation depth of the modulator based on the planar split-ring resonator array is affected by the Fabry-Perot resonances occurring within dielectric substrate when high-frequency EM field is applied. Modulation depth can be optimized by choosing proper thickness of the dielectric substrate.

Bibliography

[1] A. Taflove and S. C. Hagness, *Computational Electrodynamics: The Finite–Difference Time–Domain Method*. Boston. London: Artech House, 2000.

[2] S. J. Orfanidis, *Electromagnetic Waves and Antennas*. online, 2002.

[3] A. Jakušev, R. Čiegis, I. Laukaitytė, and V. Trofimov, "Parallelization of linear algebra algoritms using ParSol library of mathematical objects," in *Parallel Scientific Computing and Optimization. Advances and Applications. Springer Optimization and Its Applications.*, vol. 27, pp. 25–36, 2009.

[4] A. Jakušev, "Development, analysis and applications of the technology for parallelization of numerical algorithms for solution of PDE and systems of PDEs," 2007.

[5] A. Sužiedėlis, J. Gradauskas, S. Ašmontas, G. Valušis, and H. G. Roskos, "Giga- and terahertz frequency band detector based on an asymmetrically necked n-n$^+$-GaAs planar structure," *Journal of Applied Physics*, vol. 93, no. 5, pp. 3034–3038, 2003.

[6] J. G. Maloney and G. G. Smith, "The efficient modeling of thin material sheets in the finite–difference time–domain (FDTD) method," *IEEE Transactions on Antennas and Propagation*, vol. 40, no. 3, pp. 323–330, 1992.

[7] S. Ašmontas, *Electrogradient phenomena in semiconductors.* Vilnius: Mokslas, 1984.

[8] S. Ašmontas and A. Sužiedėlis, "New microwave detector," *International Journal of Infrared and Millimeter Waves*, vol. 15, no. 3, pp. 525–538, 1994.

[9] D. Seliuta, E. Širmulis, V. Tamošiūnas, S. Balakauskas, S. Ašmontas, A. Sužiedėlis, J. Gradauskas, G. Valušis, A. Lisauskas, H. G. Roskos, and K. Köhler, "Detection of terahertz/sub–terahertz radiation by asymmetrically–shaped 2DEG layers," *Electronics Letters*, vol. 40, no. 10, pp. 631–632, 2004.

[10] W. Withayachumnankul, C. Fumeaux, and D. Abbott, "Planar Array of Electric-*LC* Resonators With Broadband Tunability," *IEEE Antennas and Wireless Propagation Letters*, vol. 10, pp. 577–580, 2011.

[11] T. J. Tolmunen and M. A. Frerking, "Theoretical efficiency of multiplier devices," in *Second International Symposium on Space Terahertz Technology*, pp. 197–211, Feb. 1991.

[12] B. J. Rizzi, J. L. Hesler, H. Dossal, and T. W. Crowe, "Varactor diodes for millimeter and submillimeter wavelengths," in *Third International Symposium on Space Terahertz Technology*, pp. 73–92, 1992.

List of publications related to the dissertation

1. R. Čiegis, Ž. Kancleris, G. Šlekas, "Parallel numerical solver for modelling of electromagnetic properties of thin conductive layers", *PARALLEL PROCESSING AND APPLIED METHEMATICS, PART II Book Series: Lecture Notes in Computer Science*, Vol. **6068**, 320–329, 2010.
2. Ž. Kancleris, G. Šlekas, R. Čiegis, "Interaction Of Thin Conductive Sheets with TE_{10} Electromagnetic Wave in Rectangular Waveguide", *Proc.* 18^{th} *International conference on Microwave, Radar, and Wireless Communications MIKON-2010*, June 14-16, 2010.
3. Ž. Kancleris, G. Šlekas, R. Čiegis, "Sensitivity of Asymmetrically Necked Planar Millimeter-Wave Detectors", *IEEE Sensors Journal*, Vol. **13**(4), pp. 1143–1147, 2013.
4. Ž. Kancleris, G. Šlekas, A. Matulis, "Modeling of Two–dimensional Electron Gas Sheet in FDTD Method", *IEEE Trans. Antennas Propag.*, Vol. **61**(2), pp. 994–996, 2013.
5. G. Šlekas, Ž. Kancleris, D. Seliuta, "Tuning of resonance frequency in array of split-ring resonators in terahertz range", *Lithuanian Journal of Physics*, Vol. **54**(1), pp. 15–19, 2014.
6. R. Čiegis, A. Bugajev, Ž. Kancleris, G. Šlekas, "Parallel Numerical Algorithms for Simulation of Rectangular Waveguides by Using GPU", *PARALLEL PROCESSING AND APPLIED METHEMATICS, PART II Book Series: Lecture Notes in Computer Science*, Vol. **8385**, 301–310, 2014.

Presentations in scientific conferences

1. R. Čiegis, Ž. Kancleris, G. Šlekas, "Parallel Numerical Solver for Modelling of Electromagnetic Properties of Thin Conductive Layers", 8^{th} Int. Conf. on Parallel Processing and Applied Mathematics (PPAM2009), 2009 Sept. 11-14, Wroclaw, Poland.
2. G. Šlekas, Ž. Kancleris, R. Čiegis, "Investigation of Thin Necked Shape Conductive Structures, Interacting with TE_{10} Electromagnetic Wave in Rectangular Waveguide", 14^{th} international conference on Electronics ELECTRONICS'2010, 2010 May 18-20, Vilnus.
3. R. Čiegis, Ž. Kancleris, G. Šlekas, "Investigation of thin Conducting Sheets Interacting with TE_{10} Wave", 15^{th} International Conference Mathematical Modelling and Analysis (MMA2010), 2010 May 26-29, Druskininkai.
4. G. Šlekas, Ž. Kancleris, R. Čiegis, "Interaction of thin conductive sheets

with TE_{10} electromagnetic wave in rectangular waveguide", 18^{th} International conference on Microwave, Radar and Wireless Communications MIKON-2010, 2010 June 14-16, Vilnius.

5. G. Šlekas, Ž. Kancleris, R. Čiegis, "Modeling of terahertz radiation excited using stretched laser pulse", E2011 15^{th} International Conference on Electronics, 2011 May 17-19, Vilnius.

6. G. Šlekas, Ž. Kancleris, R. Čiegis, "Plonasluoksnio diodo jautrio dažninės priklausomybės optimizavimas baigtinių skirtumų laiko skalėje metodu", 39-oji Lietuvos nacionalinė fizikos konferencija, 2011 spalio 6-8 d., Vilnius.

7. A. Bugajev, R. Čiegis, G. Šlekas, Ž. Kancleris, "The analysis of 3D finite difference time domain calculations using CUDA", 18^{th} International Conference Mathematical Modelling and Analysis (MMA2013), 2013 May 27-30, Tartu, Estonia.

8. G. Šlekas, Ž. Kancleris, D. Seliuta, "Periodinės žiedinių rezonatorių struktūros rezonansinių savybių tyrimas", 40-oji Lietuvos nacionalinė fizikos konferencija, 2013 birželio 10-12 d., Vilnius.

9. R. Čiegis, A. Bugajev, Ž. Kancleris, G. Šlekas, "Parallel Numerical Algorithms for Simulation of Rectangular Waveguides by Using GPU", 10^{th} International Conference on Parallel Processing & Applied Mathematics (PPAM2013), 2013 Sept. 8-11, Warsaw, Poland.

10. G. Šlekas, Ž. Kancleris, D. Seliuta, "Tuning of resonance frequency in array of split ring resonators in terahertz region", 15^{th} International Symposium on Ultrafast Phenomena in Semiconductors, 2013 Aug. 25-28, Vilnius.

11. G. Šlekas, Ž. Kancleris, D. Seliuta, "Influence of Fabry-Perot resonance on modulation properties of tunable metamaterial in terahertz region", 5^{th} International Conference on Radiation interaction with materials: fundamentals and applications, 2014 May 12-15, Kaunas.

12. Ž. Kancleris, D. Seliuta, G. Šlekas, A. Urbanovič, D. Zimkaitė, "Optimization of Terahertz Metamaterial Modulator", 39^{th} International Conference on Infrared, Millimeter, and Terahertz Waves, 2014 Sept. 14-19, The University of Arizona, Tucson, AZ, USA.

Santrauka

Išvestos baigtinių skirtumų laiko skalėje (BSLS) lygtys, leidžiančios modeliuoti dvimatį laidų sluoksnį, charakterizuojamą savituoju paviršiniu laidumu. Jos patikrintos modeliuojant bangos atspindį nuo stačiakampiame bangolaidyje patalpinto dvimačių elektronų dujų sluoksnio. Pasinaudojant pasiūlytu skaičiavimo metodu, apskaičiuota elektromagnetinio lauko nuostolių bangolaidžio sienelėse priklausomybė nuo jų savitojo laidumo.

Pademonstruota, kaip BSLS skaičiavimus galima gana paprastai ir efektyviai perkelti į lygiagrečiųjų skaičiavimų įrenginius. ParSol bibliotekos panaudojimas leido gauti paspartėjimus beveik tiesiškai proporcingus bendram naudojamų kompiuterių procesorių branduolių skaičiui, kai kiekviename procesoriuje buvo aktyvūs ne daugiau nei du branduoliai. Atliekant skaičiavimus grafinėje plokštėje, kai buvo naudojama automatinio podėliavimo technologija, gauti net keleto kartų paspartėjimai lyginant su to paties uždavinio vykdymu viename centrinio procesoriaus branduolyje.

Nustatyta, kad elektrinio lauko pasiskirstymo planarinio diodo mezoje pobūdį lemia jos savitasis elektrinis laidumas σ. Kai jis yra nedidelis, mezoje dominuoja slinkties srovės, ir elektrinis laukas koncentruojasi ties GaAs–metalo sandūra. Didinant σ, elektrinio lauko pasiskirstymą sąlygoja mezos forma, kai elektrinio lauko amplitudė yra atvirkščiai proporcinga mezos pločiui tame taške. Pademonstruota, kad planarinio diodo jautrį stipriai įtakoja siaurosios bangolaidžio sienelės matmuo b. Skaičiavimų rezultatai parodė, kad bangolaidyje patalpintas planarinio diodas elgiasi panašiai kaip dipolinė antena, kurios jautris priklauso nuo dipolio ilgio. Parodyta, kad parinkus tokį b, kad santykis b/a išliktų nepakitęs, galima gauti beveik pastovią jautrio vertę, pereinant į skirtingų plačiosios sienelės a matmenų bangolaidžius. Norint, kad atspindžio koeficientas būtų mažesnis už 0.1, b/a neturėtų viršyti 0.15.

Ištirtos simetriškuose ir asimetriškuose žiediniuose rezonatoriuose (ŽR) susidarančios elektros srovės rezonansinės modos. Asimetriškuose ŽR susi-

daro nuosekli srovės moda, kai krūvininkai juda kaip LC rezonansiniame kontūre. Ši moda pasižymi aukštu rezonanso kokybės faktoriumi. Parodyta, kad ŽR masyvo filtruojančios savybės pasireiškia dėl ŽR kontūruose indukuojamų elektros srovių. Tikintis sukurti greito terahercų moduliatoriaus modelį ištirtos galimybės dinamiškai keisti ŽR masyvo filtruojamą dažnį. Pademonstruota galimybė optinio sužadinimo būdu transformuoti ŽR iš simetrinio į asimetrinį, ir taip pakeisti ŽR tekančios srovės modą bei dažnį, tokiu būdu perjungiant moduliatoriaus būseną ties ŽR rezonansiniu dažniu. Taip pat parodyta, kad integruojant aukšto dažnio varaktorių į ŽR tarpelį, galima efektyviai keisti planarinio ŽR masyvo filtruojamą dažnį. Skaitmeniškai ir eksperimentiškai nustatyta, kad ŽR masyvo moduliacijos gylį įtakoja dielektriniame padėkle aukštuose dažniuose pasireiškiantys Fabry–Perot rezonansai. Pasiūlyta kaip parenkant tinkamą padėklo storį padidinti moduliacijos gylį.